Published in final edited form as:
Ann Biomed Eng. 2012 September ; 40(9): 1903–1916. doi:10.1007/s10439-012-0568-6.

Mitochondrial Dynamics and Motility Inside Living Vascular Endothelial Cells: Role of Bioenergetics

RANDY J. GIEDT[1,2], **DOUGLAS R. PFEIFFER**[3], **ANASTASIOS MATZAVINOS**[4], **CHIU-YEN KAO**[5,6], and **B. RITA ALEVRIADOU**[1,2]

[1]Department of Biomedical Engineering, The Ohio State University, 1080 Carmack Road, Columbus, OH 43210, USA

[2]Davis Heart & Lung Research Institute, Division of Cardiovascular Medicine, Department of Internal Medicine, The Ohio State University, 473 West 12th Avenue, Columbus, OH 43210, USA

[3]Department of Molecular and Cellular Biochemistry, The Ohio State University, 1645 Neil Avenue, Columbus, OH 43210, USA

[4]Department of Mathematics, Iowa State University, Ames, IA 50011, USA

[5]Department of Mathematics, The Ohio State University, 231 West 18th Avenue, Columbus, OH 43210, USA

[6]Department of Mathematics and Computer Science, Claremont McKenna College, 850 Columbia Avenue, Claremont, CA 91711, USA

Abstract

The mitochondrial network is dynamic with conformations that vary between a tubular continuum and a fragmented state. The equilibrium between mitochondrial fusion/fission, as well as the organelle motility, determine network morphology and ultimately mitochondrial/cell function. Network morphology has been linked with the energy state in different cell types. In this study, we examined how bioenergetic factors affect mitochondrial dynamics/motility in cultured vascular endothelial cells (ECs). ECs were transduced with mitochondria-targeted green fluorescent protein (mito-GFP) and exposed to inhibitors of oxidative phosphorylation (OXPHOS) or ATP synthesis. Time-lapse fluorescence videos were acquired and a mathematical program that calculates size and speed of each mitochondrial object at each time frame was developed. Our data showed that inner mitochondrial membrane potential ($\Delta\Psi_m$), ATP produced by glycolysis, and, to a lesser degree, ATP produced by mitochondria are critical for maintaining the mitochondrial network, and different metabolic stresses induce distinct morphological patterns (e.g., mitochondrial depolarization is necessary for “donut” formation). Mitochondrial movement, characterized by Brownian diffusion with occasional bursts in displacement magnitude, was inhibited under the same conditions that resulted in increased fission. Hence, imaging/mathematical analysis shed light on the relationship between bioenergetics and mitochondrial network morphology; the latter may determine EC survival under metabolic stress.

Address correspondence to B. Rita Alevriadou, Departments of Biomedical Engineering and Internal Medicine, The Ohio State University, 473 West 12th Avenue, DHLRI 607, Columbus, OH 43210, USA. alevriadou.1@osu.edu or rita.alevriadou@osumc.edu.

ELECTRONIC SUPPLEMENTARY MATERIAL
The online version of this article contains supplementary material, which is available to authorized users.

Key Terms

Mitochondrial fusion/fission; Mitochondrial motility; Endothelial function; Fluorescence microscopy; Digital image processing; Mathematical analysis; Object tracking

INTRODUCTION

Mitochondria are dynamic organelles that undergo cycles of fusion and fission. An imbalance of these two processes alters mitochondrial morphology: Disruption of fusion or enhancement of fission causes the normal, tubular mitochondrial network to initially acquire a truncated and eventually a fragmented phenotype. Conversely, disruption of fission or enhancement of fusion generates elongated tubules.[8,30–31] Four GTPases regulate mitochondrial dynamics in mammals: Dynamin-related protein 1 (Drp1) is essential for fission, and the mitofusins (Mfn1, Mfn2) and optic atrophy 1 (Opa1) are essential for fusion.[24,44] The importance of maintaining mitochondrial network morphology is demonstrated by the fact that mice lacking the fusion machinery are embryonic lethal, and mutations in fusion/fission proteins have been implicated in neurological and vascular diseases.[7] Upon cell exposure to apoptotic stimuli, Drp1 is transported to mitochondria, where it oligomerizes at fission sites and interacts with Bax/Bak on the outer membrane resulting in membrane permeabilization and cytochrome c release/apoptosis.[4,49] In transformed cells or primary neurons exposed to apoptotic stimuli, mitochondria underwent increased fission, which was prevented by expression of a dominant-negative form of Drp1. Fission prevention prolonged cell survival suggesting that uninhibited fission leads to apoptosis.[14,28] Furthermore, mitochondrial elongation through hyperfusion was shown to regulate cell cycle progression,[33] senescence,[48] and cell responses to selective stimuli, such as amino acid deprivation.[37,45]

Mitochondrial network morphology is determined not only by dynamics, but also by the organelle motility. Mitochondrial movement has been studied extensively in neurons, where mitochondria are transported along microtubules utilizing ATP-dependent motor proteins. For motion in an anterograde fashion, they utilize the motor protein kinesin, whereas, for motion in a retrograde fashion, they use dynein.[15,23] Kinesin binds to mitochondria through an adaptor protein complex formed of Miro and Milton. In the presence of high calcium (Ca^{2+}) levels, Ca^{2+} binds to Miro and dissociates kinesin from microtubules, resulting in stationary mitochondria.[38] Segregation of mitochondria at high Ca^{2+} sites allows for increased Ca^{2+} buffering and increased ATP production to help pump Ca^{2+} out of the cell.[47] In epithelial cells, tracking of individual mitochondria demonstrated that they mostly undergo Brownian motion (wiggling around their initial position), but some demonstrate random bursts in their speed corresponding to motor-driven, directional movement.[39]

Although mitochondria share similar properties in most tissues, their morphology and dynamic behavior vary among cell types, and the proteins that regulate mitochondrial dynamics and motility can be cell type-specific.[27] Changes in bioenergetics are expected to affect mitochondrial network morphology by modulating the activity of mitochondrial fusion/fission and motility proteins due to altered ATP/GTP levels and upstream signaling cascades (the latter may result in post-translational modifications of the mitochondrial remodeling proteins).[1,40] In various cell lines and primary human fibroblasts, low inner mitochondrial membrane potential ($\Delta\Psi_m$) and low ATP levels were the necessary conditions, and high mitochondrial reactive oxygen species (mtROS) were important, for fission initiation.[1,19,40]

Our aim is to delineate the bioenergetic modulation of mitochondrial dynamics and motility in human vascular endothelial cells (ECs). Altered dynamic behavior of the EC mitochondria may contribute to mitochondrial and, ultimately, EC dysfunction, which is the hallmark of many vascular diseases/conditions, such as atherosclerosis, diabetes and ischemia/reperfusion injury.[46] Earlier studies by us and others[16,26] examined the EC mitochondrial morphology and showed that EC exposure to oxidative stress leads to increased fission, but did not investigate the role of bioenergetics in the mitochondrial dynamic behavior. Hence, in this study, cultured human umbilical vein ECs (HUVECs) transduced with mitochondria-targeted green fluorescent protein (mito-GFP) were treated with inhibitors of oxidative phosphorylation (OXPHOS) or a glycolysis inhibitor followed by time-lapse fluorescence microscopy. A mathematical/computational program was developed to track the shape/size and speed of individual mitochondria in video frames, thus, allowing for counting the number of fusion and fission events in a certain time period, calculating the mean squared displacement for mitochondrial objects and estimating an apparent diffusion coefficient for each condition tested. Our analysis revealed that $\Delta\Psi_m$, ATP produced by glycolysis, and, to a lesser extent, ATP produced by mitochondria are all required to maintain the original balance between fusion/fission (and the network in its tubular conformation). In the case of depolarized mitochondria or upon glycolysis inhibition, there was a transient period where the fission rate increased and the fusion rate decreased before they reached equal, but lower than their original, values, leading to fragmentation of the network. Under these conditions, mitochondrial motility, as measured by the percentage of mitochondria undergoing “random steps” in displacement magnitude, also declined. Only in the case of pronounced mitochondrial depolarization, did a significant percentage of mitochondria acquire a characteristic “donut” shape. In summary, use of imaging/mathematical techniques allowed us to quantitatively characterize the dynamic behavior of fluorescently-labeled mitochondria in ECs exposed to bioenergetic stress.

MATERIALS AND METHODS

HUVEC Culture and Treatment

Pooled primary HUVECs (Cambrex, East Rutherford, NJ) were grown in complete EC growth medium (Cell Applications, San Diego, CA) in a tissue culture incubator. ECs were seeded on glass-bottomed 35 mm culture dishes (0.17 mm thickness coverslips at the bottom; MatTek, Ashland, MA) and cultured in complete medium. At ~70% confluence, ECs (passage 3–8) were incubated with 3% v/v of the Organelle Lights mitochondria-targeted green fluorescent protein (mito-GFP) BacMam reagent, reconstituted according to the manufacturer’s guidelines (O36210, Invitrogen, Carsbad, CA), in complete medium for 24 h. Alternatively, some ECs were incubated with the CellLight mito-red fluorescent protein (mito-RFP) BacMam reagent (C10601, Invitrogen). Each reagent contains a baculovirus that, upon entry into the cells, directs the expression of a fluorescent protein to mitochondria via the leader sequence of E1α pyruvate dehydrogenase. ECs were kept in complete medium for another 24 h until confluence followed by equilibration in a HEPES-buffered saline solution (HBSS; 140 mM NaCl, 5 mM KCl, 1 mM $MgCl_2 \cdot 6H_2O$, 1 mM $CaCl_2 \cdot 2H_2O$, 10 mM D-glucose, 10 mM HEPES, pH 7.4) containing 1% w/v bovine serum albumin (Sigma, St Louis, MO) for 1 h to establish a baseline and limit responses due to serum and growth factors. ECs were treated with saturating concentrations of the following compounds for 30 min to study the role of bioenergetic stress on mitochondrial morphology (Fig. 1 shows schematically the target sites of each compound in the OXPHOS and glycolysis pathways):

a. Control: Some ECs were incubated in HBSS in the presence of DMSO (amounts equivalent to those that the cells were exposed to for treatments b, c and d; stocks

of those compounds were made in DMSO) or in the absence of DMSO for treatments e and f.

b. An OXPHOS uncoupler, carbonylcyanide-p-trifluoromethoxyphenylhydrazone (FCCP): Some ECs were treated with either a low FCCP concentration, 0.5 μM (FCCP-L), or a high one, 5 μM (FCCP-H); the latter concentration is known to cause maximal dissipation of the $\Delta\Psi_m$.[35]

c. An inhibitor of OXPHOS complex III, antimycin A: Some ECs were treated with antimycin A at 10 μM; known to cause pronounced mitochondrial depolarization in ECs by 30 min.[16]

d. An inhibitor of the mitochondrial ATP synthase (OXPHOS complex V), oligomycin: Oligomycin at 5 μM was used to block the mitochondria-specific ATP production.[19]

e. An inhibitor of glycolysis, 2-deoxy-D-glucose (2DG): Replacement of D-glucose in HBSS by 2DG (10 mM), a glucose derivative that is internalized and phosphorylated but cannot undergo glycolysis, was used to inhibit cytosolic ATP production.[19,40]

f. Fetal bovine serum: Serum (10% v/v; Invitrogen) was added to HBSS in some culture dishes. Since serum contains insulin and growth factors, it activates the serine/threonine kinase Akt resulting in increased glycolysis/OXPHOS and elevation of the intracellular ATP levels.[18,20]

Digital Video Acquisition and Image Processing

After equilibration in HBSS, each culture dish with an EC monolayer was placed on a motorized stage (Prior Scientific, Rockland, MA), kept at 37 °sC, of a TE2000 Nikon microscope (Nikon Instruments, Melville, NY) equipped with a CCD camera (Digital Sight DS-Qi1Mc, Nikon) for fluorescence imaging (90x magnification; GFP: 485 nm excitation/ 520 nm emission; RFP: 514 nm excitation/585 nm emission). Control videos were collected for 1–3 min at 1 Hz from selected locations on the coverslip using Nikon Elements. Either one of the compounds (a–d, f) was added to HBSS or HBSS was gently replaced with HBSS containing 2DG, and 1 min videos were collected from the same locations at 5 and 30 min following compound addition or HBSS replacement. When necessary, we would focus during the short recording periods; no system drift was observed in the XY plane relative to a scratch on the dish bottom. Videos were manually cropped into smaller recordings corresponding to ~1/10 of the area covered by the original images. These regions of interest were selected closer to the cell periphery to avoid the mitochondria in the overcrowded area surrounding the nucleus.[43] A macro in ImageJ[9] was applied on each cropped video to contrast enhance each time frame in the video at 0.5% of saturation levels. Contrast enhanced images underwent convolution with a Laplacian kernel to reveal structures defined by a rapid fluorescence intensity change. The operator C is given by

$$C(x,y)=\sum_{s=-a}^{a}\sum_{t=-b}^{b}K(s,t)I(x-s,y-t) \quad (1)$$

where I(x, y) and C(x, y) denote the intensity of pixel (x, y) in the original and convolved images, respectively, and parameters a and b depend on the size of the Laplacian kernel K.[21] In our case, a 5×5 isotropic kernel (with a=2, b=2)[17] was found to produce optimal results

$$K = \begin{pmatrix} -1 & -1 & -1 & -1 & -1 \\ -1 & -1 & -1 & -1 & -1 \\ -1 & -1 & 24 & -1 & -1 \\ -1 & -1 & -1 & -1 & -1 \\ -1 & -1 & -1 & -1 & -1 \end{pmatrix} \quad (2)$$

Following convolution, image speckling was filtered using a bandpass filter based on the Fast Fourier Transform algorithm.[17] Briefly, each image was transformed into the frequency domain, large structures were filtered down to 100 pixels, small structures were filtered up to 3 pixels and the image was subsequently returned to the spatial domain. Otsu's algorithm, which functions by iteratively minimizing the difference between the weighted sums of the foreground and background pixel intensity variances, was utilized with a slight variable offset to reduce each filtered image into a thresholded, binary form consisting of mitochondria (white) and background (black).[17] Fig. 2a shows the processing sequence of a video frame that contains a single cell starting from the original image and finishing with a binary image suitable for object tracking.

To determine the height of the mitochondrial network, some control EC monolayers were observed using confocal fluorescence microscopy at 100x magnification (Olympus Fluoview 1000, Center Valley, PA). 41 optical Z slices were acquired every 0.5 μm covering every cell in the monolayer. The Nikon Elements software was employed to create 3D reconstructions (Z-stacks) and XZ and YZ projections of those Z-stacks.

Analysis of Mitochondrial Dynamics

A Matlab program (MathWorks, Natick, MA) was created to track objects from binarized videos. Each video is represented as a matrix with the size (m1, m2, m3) corresponding to the x and y dimensions in 2D, as well as the frame number (time) in the z direction. Connected objects were labeled in 3D using the Matlab function "bwlabeln",[22,42] an algorithm which first run length encoded each image. Preliminary values were assigned to regions on the coded image and an equivalence table was created to resolve conflicting labeling due to labeling propagation (assigning integer values to non-zero areas of the binary image). Conflicts are inherent in this process, when a single region has branching in its top areas (displaying two disparate regions where only one exists). Final labels were assigned based on 6-point (for 3D labeling) connectivity. This process results in a label matrix, L3, with the same size as the (m1, m2, m3), containing labels for the connected components in the input image. The elements of L3 are integer values ≥0: Pixels labeled 0 are the background; pixels labeled 1 make up one object; pixels labeled 2 make up a second object; etc. That means that some mitochondria are recognized as a single object in 3D, as long as they merge at a certain time in the video. Fig. 2b shows a simplified example of a 3D label matrix (broken down to 2D, time labeled segments) with a size of (5,5,4). Images at each time frame were labeled using a "bwlabel" algorithm with 4-point connectivity to identify the connected regions. This creates a second label matrix, L2. Based on 2D labeling, we can identify the centroid of each connected region (shown as black dots in Fig. 2b) and match the regions in consecutive time frames by referring to their L3 index. Thus, we maintained label consistency for each object across time (using the L3 matrix) and extracted properties, such as size, object centroids and total number of objects in each 2D area (using the L2 matrix). In the event of fission, tracking of the previous region was concluded at that time point and tracking for the new regions started. In the event of fusion, tracking of the previous regions ended and tracking for a new object started. In order for a fragment to be counted, it was required to exist separately from other fragments for ≥3 s. Regions were

color coded according to their interactions (i.e., interacting objects were identically pseudo colored) for visual confirmation of the events occurring in the video (Fig. 2b).

For analysis of mitochondrial "donut" formation, time frames were obtained from videos and processed as described above. Donuts were identified using the function "bwlabel" in Matlab, as well as "bwboundaries", which isolated those objects found with "bwlabel" with a closed hole in their center. The above functions then displayed only those objects with enclosed areas and a size between 0.2 μm^2 and 2 μm^2. Donut counts were verified by visual inspection.

Analysis of Mitochondrial Motility

For mitochondrial motility analysis, object displacement $\delta(t)$ at each time point was calculated

$$\delta(t)=r(t_0+t)-r(t_0) \tag{3}$$

where $r(t_0)$ represents the position of an object at time t_0 (because videos were taken at 1 Hz, the time step is 1 s). To calculate the speed at each time point, we divided the magnitude of the displacement vector by the time step. Net displacement was calculated by taking the difference between the object's current position and its origin (position at $t_0=0$). Furthermore, the mean squared displacement (MSD; a measure of the average distance traveled by an object) was calculated for each object[2,36,41]

$$MSD=\langle|\delta(t)|^2\rangle=\langle|r(t_0+t)-r(t_0)|^2\rangle \tag{4}$$

where <…> denotes a time average. Theoretically, the ensemble average MSD varies with time as

$$Average\ MSD \propto t^{a} \tag{5}$$

where $0<\alpha<2$. The mode of transport that the particle undergoes is classified according to the value of α: $\alpha=1$ indicates Brownian diffusion, $\alpha<1$ indicates confined diffusion and $\alpha>1$ indicates directed diffusion, with $\alpha=2$ indicating directed motion with no diffusion. In the case of Brownian diffusion in a 2D system, the average MSD is expected to increase linearly with time, and the slope is related to the diffusion coefficient D as follows

$$Average\ MSD=4Dt \tag{6}$$

In this study, the α values were calculated by conducting a curve fit using a least squares method of linear regression to fit the average MSD data to Eq. (5) for each condition tested. In the case of Brownian diffusion, a second linear curve fit was conducted according to Eq. (6), to determine the D value. In order to quantify the percentage of objects that undergo a burst in displacement magnitude ("step" motion) per min of video recording, we arbitrarily set a threshold of net displacement as a level one standard deviation above the average net displacement (from the origin) within 1 min of recording of mitochondrial motion in control cells; this same standard was applied across all conditions.

Statistical Analysis

Data from counts of total objects or objects undergoing random steps, as well as fusion/fission rates, were expressed as mean±SE of $n\geq3$ independent experiments. Differences

among treatments were determined using one-way ANOVA followed by Bonferroni's test. Regarding object lengths, a mixed model treated each experiment within treatment as a random variable to take the correlation of object lengths for each experiment into account. Hypothesis testing was conducted using linear contrasts of parameter estimates, and multiple comparisons were adjusted for using Holm's method.[12] P values <0.05 were considered significant.

RESULTS

Mitochondrial Morphology Alterations due to Bioenergetic Stress

We first quantified changes in EC mitochondrial morphology at the end of 30 min treatments compared to their respective controls. Characteristic binary images at 30 min from each treatment demonstrated that the balance between fusion/fission was tipped markedly towards fission in the presence of FCCP-H or antimycin A; to a lesser extent, in the presence of oligomycin or 2DG; and insignificantly, in the presence of FCCP-L (Fig. 3a). The number of objects, expressed as percent change compared to control (control ECs have on average ~200 mitochondrial objects each), increased significantly in cells treated with FCCP-H, antimycin A, oligomycin or 2DG (Fig. 3b). Box plots showing the $90^{th}/10^{th}$ and $25^{th}/75^{th}$ percentiles and medians of mitochondrial length were plotted for each treatment, and FCCP-H, antimycin A and 2DG were found to cause the most extensive object shortening (Fig. 3c). These data suggest that $\Delta\Psi_m$ and, in particular, ATP produced by glycolysis are critical in maintaining the balance between fusion/fission in ECs. Finally, ECs in the presence of serum showed a small, non-significant decrease in the number of objects and a non-significant increase in object length compared to control (Fig. 3a–c) suggesting that increased cytosolic ATP levels may tip the balance towards fusion.

To analyze the effect of each treatment on donut formation, donuts were identified, as described in Analysis of Mitochondrial Dynamics, and shown in Fig. 4a for a characteristic original image of a cell with donut-shaped mitochondria (a grayscale version of Fig. 4 is included in supplemental material). Donut formation was expressed as a percentage of total objects and occurred exclusively in the presence of either FCCP-H or antimycin A (Fig. 4b), suggesting that $\Delta\Psi_m$ dissipation is required for donut formation. Donuts had an average diameter of 0.4 μm and never exceeded a diameter of 0.8 μm (>100 donuts were analyzed). No donuts formed in the presence of FCCP-L suggesting that depolarization needs to reach a certain level before the mitochondria acquire this particular morphology.

Control EC Mitochondria are Highly Dynamic

Fig. 5 shows the results from executing the Matlab program (demonstrated in Fig. 2b) to a 90 s control video of a control cell transduced with mito-GFP. Time frames at 0 and 90 s from that video, each with a cropped area of analysis (white box), are shown in Fig. 5a (see supplementary material for the corresponding movie). Fig. 5b shows, on the top row, contrast-enhanced time frames of the cropped area in 10 s intervals, and, on the bottom row, the corresponding Matlab outputs. In the latter, mitochondria were color coded according to interactions for visual confirmation of automated results: Identically colored objects interact with each other at some point in the video, whereas dissimilar color indicates no interaction with objects of other colors. Also on the bottom row, arrows and arrowheads were added after Matlab analysis to indicate individual fission and fusion events, respectively, and demonstrate the dynamic nature of the EC mitochondrial reticulum.

Alterations in Mitochondrial Dynamics and Motility due to Bioenergetic Stress

Besides quantifying mitochondrial morphology at the 30 min time frame, dynamic mitochondrial behavior was studied by executing the Matlab program and measuring the

rates of fusion and fission events at 0, 5, and 30 min of treatment. In the case of FCCP treatment, each concentration tested caused the fission rate to become significantly higher than the fusion rate by 5 min of treatment (rates were not significantly different in control cells), thus, tipping the balance towards fission; both fission and fusion rates at 5 min were significantly different from the rates in the corresponding control in the presence of FCCP-H (Fig. 6a). By 30 min, the fission and fusion rates for both FCCP-L and -H reached a new equilibrium with each other, but significantly lower overall values compared to the corresponding control; FCCP-H caused the most dramatic decline in rates (Fig. 6a). Similarly, antimycin A, oligomycin and 2DG caused the fusion/fission rates at 30 min to attain a new equilibrium at significantly lower levels, whereas serum caused significant increases in the fusion/fission rates compared to control (Fig. 6b). FCCP-H, antimycin A and 2DG were the most effective in diminishing the dynamic behavior of the mitochondrial network suggesting that the fusion/fission machinery mainly requires $\Delta\Psi_m$ and cytosolic ATP.

For mitochondrial motility analysis, centroids were tracked over time for each object in a cropped video, as shown in Fig. 7a. The movement of randomly selected objects A and B, whose centroids were tracked, was characterized by calculating object speed and net displacement at each time point during 180 s of video (Fig. 7b and c, respectively; blue dotted line for A; red solid line for B). In general, the calculated speeds at each time point varied from 0.01 up to 2 μm/s, but the vast majority of mitochondria moved with speeds <0.5 μm/s. The average net displacement/min (>100 objects) in control cells was estimated to be 0.31 μm with a standard deviation of 0.54 μm, and, thus, objects that moved outside of a 0.85 μm boundary from their origin per min of recording were identified as undergoing bursts or steps in displacement magnitude. For example, between 20–50 s, object B showed increased speeds resulting in a net displacement of >0.85 μm at later times (indicated by the horizontal dotted line in Fig. 7c) and, thus, exhibited this step-like motion. As expected, the MSD vs. time plots for the two objects studied showed a large rise in the MSD of B between 20–50 s, whereas the MSD of A increased linearly with time (Fig. 7d).

Fig. 8a shows experimental MSD vs. time profiles for 10 mitochondrial objects in a control cell demonstrating the heterogeneity in their movement. However, when the average MSD was calculated (Cntrl panel of Fig. 8b) and fitted to Eq. (5), the α value was close to 1, indicating that, on average, the mitochondria in control ECs undergo Brownian diffusion. Following a linear curve fit (the eq. of the linear curve fit and the goodness-of-fit test are shown), D was estimated: D for control = 3×10^{-3} $\mu m^2/s$. When the above analysis was performed in treated ECs, it was found that the mitochondria exhibit free diffusion during each treatment studied, and the D values were: D for FCCP-H = 0.3×10^{-3}; D for antimycin = 0.3×10^{-3}; D for oligomycin = 1.5×10^{-3}; D for 2DG = 1×10^{-3}; and D for serum = 6.5×10^{-3} (in units of $\mu m^2/s$).

The percentage of objects that underwent Brownian diffusion with interspersed “random steps” (an index of motility) was then calculated, based on the threshold posed on the magnitude of net displacement/min, and was found to significantly decrease in ECs exposed to all treatments compared to control (Fig. 9a). On the contrary, serum addition significantly increased object participation in diffusion with bursts in displacement magnitude (Fig. 9a). To probe for a correlation between mitochondrial motility and size, the percentage of objects exhibiting “random steps” were binned by size for each condition tested; only control, FCCP-H and serum are shown (Fig. 9b). Both the control and FCCP-H, despite different mitochondrial morphologies and extents of participation in “random steps”, primarily had their smallest mitochondria undergo bursts in displacement. On the contrary, the majority of objects that underwent “random steps” in serum-treated ECs were large mitochondria (Fig. 9b). Taken together, our results suggest that the same conditions that favor fission, in

general, limit motility, and there is no clear relationship connecting size and motility. Last, donuts showed no participation in “random steps” (data not shown), as did the majority of the objects in FCCP-H- and antimycin A-treated cells.

Control EC Mitochondrial Morphology in 3D

Since the mathematical analysis of mitochondrial shape and motion was done in 2D, one concern would be related to the microscope resolution (in the z direction) and object movements out of the focal plane. To address this concern, control ECs transduced with mito-GFP were imaged using confocal fluorescence microscopy (100x magnification). Fig. 10 shows a representative 3D reconstruction (Z-stack) from a control EC; 41 optical Z slices were acquired every 0.5 μm covering a total height of 20 μm. As you can see from the XZ and YZ projections of the Z-stack, the height of the mitochondrial network close to the cell periphery (from where regions were cropped for 2D analysis) is ≤4 μm. For our 2D wide-field fluorescence microscopy, we used a 60x objective with 0.7 numerical aperture (and an additional x1.5 optical magnification bringing the total magnification to 90x). With this objective, we have >4 μm out of focus light (depth of focus), so if a mitochondrial object was moving above or below the focal plane, we would see it become blurry. However, no parts of mitochondria become blurry throughout our videos (as can be seen in the movie in supplemental material), indicating that objects are not moving out of focus. Locations where darkness was present were, therefore, indicative of space between objects following fission events.

DISCUSSION

Using novel digital image processing/single particle tracking techniques, we characterized mitochondrial dynamics and motility inside live cultured HUVECs exposed, or not, to bioenergetic stress. Single particle tracking of subcellular structures in live cell imaging has, as a key goal, the establishment of correspondence between particle images in a time sequence of frames that is complicated by high particle density, particle motion and particle merging/splitting.[25] The highly acclaimed study by Jaqaman et al.[25] used a combinatorial optimization algorithm to link particles between consecutive frames and then link the resulting track segments into complete trajectories. Instead, we linked particle images with same index in 3D labeling (the 3rd dimension being time) by tracking their centroid coordinates; this resulted in a simple algorithm robust enough for our application (taking into consideration that the areas analyzed were chosen so as to avoid the mitochondrially dense, perinuclear region). Our study is the first to quantitatively examine all of the parameters that characterize mitochondrial dynamic behavior in HUVECs. We showed that mitochondria in control ECs continuously undergo fusion/fission (~65 events/min for 10^3 objects; Fig. 6a) and their motion can be characterized as Brownian diffusion interspersed with random bursts in magnitude of displacement (~28% of objects travel >0.85 μm from their original position per min of tracking; Figs. 8 and 9a). From analysis of average MSDs, the value of D that describes mitochondrial diffusion in an isotropic medium (cytosol) was extracted.[36,41] D in control ECs was 3×10^{-3} μm^2/s; it was half/one third in ECs treated with oligomycin or 2GD, respectively, and was an order of magnitude smaller in ECs treated with either FCCP-H or antimycin, suggesting that cell exposure to bioenergetic stress limits the mitochondrial diffusivity. Jendrach et al.[26] reported an average count of fusion/fission events in HUVECs that is, at least, an order of magnitude lower than ours. The discrepancy may be due to the fact that they used mitotracker for mitochondrial staining and confocal microscopy for visualization; slow acquisition and high intensity laser excitation may have precluded accurate measurements of motile mitochondria without occurrence of photobleaching or phototoxicity. 3D reconstruction from control ECs transduced with mito-GFP was used in this study to determine the height of the mitochondrial network close to the

cell periphery (Fig. 10) and, thus, defend the analysis of mitochondrial dynamics/motility using wide-field fluorescence microscopy.

To elucidate the bioenergetic control of mitochondrial dynamics, we modulated OXPHOS function in ECs by uncoupling OXPHOS with FCCP, inhibiting the respiratory chain with antimycin A, and blocking mitochondrial and cytosolic ATP synthesis by oligomycin and 2DG, respectively (Fig. 1). Since saturating concentrations of FCCP and antimycin A caused extensive fragmentation followed by 2DG and oligomycin (Fig. 3), we concluded that primarily, $\Delta\Psi_m$ and secondarily, ATP synthesis are important for maintaining the balance between fusion/fission. Similar studies in different cell lines showed that OXPHOS inhibitors or inhibitors of ATP synthesis caused mitochondrial network fragmentation, but could not infer whether fragmentation was due to increased fission, decreased fusion, or both.[1,40] Use of our Matlab algorithm allowed us to count fission/fusion events during EC exposure to metabolic stress, and showed that $\Delta\Psi_m$, ATP synthesis by glycolysis and, to a lesser extent, ATP synthesis by mitochondria are critical for maintaining the fusion and fission activities at control levels (Fig. 6). The relative effects of 2DG and oligomycin on dynamics agree with the fact that ECs are highly glycolytic and 2DG obliges the cells to rely on OXPHOS resulting in dramatic drops in cellular ATP compared to oligomycin.[10] On the contrary, human fibroblasts upon 2DG treatment are known to retain their filamentous mitochondria confirming that the same metabolic stress elicits distinct mitochondrial responses in different cell types.[19]

The intracellular signaling mechanisms that mediate the decrease in fusion and increase in fission following cell exposure to bioenergetic stress have not been fully elucidated. However, since all GTPases involved in fusion are either in the cytosol or the mitochondrial intermembrane space, it is expected that they will be modulated by cytosolic GTP levels, which are proportional to cytosolic ATP levels.[40] Specifically for Opa1, $\Delta\Psi_m$ dissipation is paralleled by proteolytic cleavage of long Opa1 isoforms to short ones that are incapable of supporting fusion.[13] Although, in this study, we attribute the regulation of mitochondrial dynamics to the two bioenergetic parameters $\Delta\Psi_m$ and ATP, it should be mentioned that these are interconnected with additional parameters, such as the levels of mitochondrial Ca^{2+} and ROS. It is possible that, upon cell stimulation, Ca^{2+} homeostasis is disturbed and increases in cytosolic Ca^{2+} levels, via activation of kinases and/or phosphatases, result in posttranslational modifications of Drp1 that, collectively, increase its activity and, thus, enhance fission.[5] Decreased cellular ATP levels, in particular, lead to an increase in cytosolic Ca^{2+}, due to lack of ATP for the pumps that transport Ca^{2+} out of the cell. Cytosolic Ca^{2+} overload may increase the levels of Ca^{2+} inside the mitochondria resulting in mtROS generation.[3] MtROS, via ROS-induced ROS release, is known to lead to coordinated ROS production from other cellular ROS sources, such as NADPH oxidase or xanthine oxidase. On the other hand, cytosolic ROS can oxidize Ca^{2+} transport systems, such as the channels releasing Ca^{2+} from intracellular stores, and, thus, increase cytosolic and mitochondrial Ca^{2+} levels.[3] In an earlier study,[16] we showed that ROS, including mtROS, via Drp1 activation play an important role in EC mitochondrial fission, confirming the complex relationship between bioenergetics and mitochondrial dynamics.

In a study of mitochondrial motility in neurons,[15] the average speeds reported (0.3–0.5 μm/s) were in the same range with those estimated by us for EC mitochondria. An apparent D value was reported for neuronal mitochondria exhibiting Brownian motion (4×10^{-3} μm^2/s)[34] that is very close to the D value estimated in this study. Object participation in “random steps” under different treatments (Fig. 9a) paralleled the dynamic changes in fusion/fission (Fig. 6a and b) and almost paralleled the final morphological changes (Fig. 3b and c) confirming that mitochondrial motility is important for fusion/fission. Overall, the same bioenergetic factors that enhanced fission led to decreased motility. Decreased ATP levels

probably limit motility via ATP starvation of the ATP-dependent motor proteins and/or action modulation of the Ca^{2+}-dependent Miro, segregating mitochondria at sites of high Ca^{2+} concentrations.[6,47] Mfn2 was recently shown to interact with Miro and be necessary for mitochondrial transport, providing a direct connection between dynamics and motility.[32] Although fragmentation occurs under the same conditions that limit motility, when we examined the size distribution of mobile mitochondria, surprisingly we found a preference for the smaller mitochondria to undergo bursts in displacement (Fig. 9b). The molecular mechanisms that determine the movement of these smaller mitochondria are currently unknown; it could be the local concentration gradients of Ca^{2+}, ATP and ROS or it could be the interactions between particular motor proteins and cytoskeletal elements. In contrast, serum treated cells exhibited steps in displacement primarily by large mitochondria (Fig. 9b), which agrees with the formation of hyperfused mitochondria (Fig. 3b and c) and the increased percentage of mitochondria participating in random steps (Fig. 9a). Increased ATP levels in cells exposed to serum[20] probably favor both the mitochondrial hyperfusion and the increased motility.

One of the most interesting observations, never before reported for ECs, is the formation of donuts by abnormal fusion only under conditions that dissipate the $\Delta\Psi_m$ (Fig. 4). Studies of donuts following mitochondrial depolarization in fibroblast and cardiomyoblast cell lines showed that donut formation follows mitochondrial detachment from microtubules, opening of the mitochondrial permeability transition pore and swelling.[11,29] Donuts were more competent to regain $\Delta\Psi_m$ after removal of the bioenergetic stress, suggesting that this distinct morphology may serve as a cell protective mechanism.[27] In summary, this study quantitatively characterized the role of bioenergetic factors, in particular $\Delta\Psi_m$ and ATP, on EC mitochondrial dynamics/motility. Since more and more links are coming up connecting mitochondrial morphology with cell apoptosis/death[24] and EC survival is of major importance in cardiovascular health, understanding the mechanisms that regulate EC mitochondrial dynamics/motility warrants further research.

Supplementary Material

Refer to Web version on PubMed Central for supplementary material.

Acknowledgments

The authors would like to thank Mr. C. J. Lloyd, undergraduate researcher, for his assistance with data analysis. This work was supported by National Institutes of Health (NIH) grant HL106392 to B. R. Alevriadou and an American Heart (AHA) predoctoral fellowship to R. J. Giedt. D. R. Pfeiffer was supported by the Ellie Kovalck Charitable Trust. A. Matzavinos was supported in part by the Mathematical Biosciences Institute at the Ohio State University and National Science Foundation (NSF) grant DMS-093164. C.-Y. Kao was supported in part by NSF grant DMS-0811003 and an Alfred P. Sloan Fellowship.

References

1. Benard G, Bellance N, James D, Parrone P, Fernandez H, Letellier T, Rossignol R. Mitochondrial bioenergetics and structural network organization. J Cell Sci. 2007; 120:838–848. [PubMed: 17298981]
2. Bomzon Z, Knight MM, Bader DL, Kimmel E. Mitochondrial dynamics in chondrocytes and their connection to the mechanical properties of the cytoplasm. Journal of Biomechanical Engineering. 2006; 128:674–679. [PubMed: 16995753]
3. Brookes PS, Yoon Y, Robotham JL, Anders MW, Sheu SS. Calcium, ATP, and ROS: a mitochondrial love-hate triangle. Am J Physiol Cell Physiol. 2004; 287:C817–833. [PubMed: 15355853]
4. Cassidy-Stone A, Chipuk JE, Ingerman E, Song C, Yoo C, Kuwana T, Kurth MJ, Shaw JT, Hinshaw JE, Green DR, Nunnari J. Chemical inhibition of the mitochondrial division dynamin reveals its role

in Bax/Bak-dependent mitochondrial outer membrane permeabilization. Dev Cell. 2008; 14:193–204. [PubMed: 18267088]

5. Chang CR, Blackstone C. Dynamic regulation of mitochondrial fission through modification of the dynamin-related protein Drp1. Ann N Y Acad Sci. 2010; 1201:34–39. [PubMed: 20649536]
6. Chang KT, Niescier RF, Min KT. Mitochondrial matrix Ca^{2+} as an intrinsic signal regulating mitochondrial motility in axons. Proc Natl Acad Sci U S A. 2011; 108:15456–15461. [PubMed: 21876166]
7. Chen H, Chan DC. Emerging functions of mammalian mitochondrial fusion and fission. Hum Mol Genet. 2005; 14(Spec2):R283–289. [PubMed: 16244327]
8. Chen H, Chomyn A, Chan DC. Disruption of fusion results in mitochondrial heterogeneity and dysfunction. J Biol Chem. 2005; 280:26185–26192. [PubMed: 15899901]
9. Collins TJ. ImageJ for microscopy. Biotechniques. 2007; 43:25–30. [PubMed: 17936939]
10. Culic O, Gruwel ML, Schrader J. Energy turnover of vascular endothelial cells. Am J Physiol. 1997; 273:C205–213. [PubMed: 9252458]
11. De Vos KJ V, Allan J, Grierson AJ, Sheetz MP. Mitochondrial function and actin regulate dynamin-related protein 1-dependent mitochondrial fission. Curr Biol. 2005; 15:678–683. [PubMed: 15823542]
12. Demidenko, E. Mixed Models: Theory and Applications (Wiley's Series in Probability and Statistics). John Wiley & Sons, Inc; Hoboken, NJ: 2004.
13. Duvezin-Caubet S, Jagasia R, Wagener J, Hofmann S, Trifunovic A, Hansson A, Chomyn A, Bauer MF, Attardi G, Larsson NG, Neupert W, Reichert AS. Proteolytic processing of OPA1 links mitochondrial dysfunction to alterations in mitochondrial morphology. J Biol Chem. 2006; 281:37972–37979. [PubMed: 17003040]
14. Frank S, Gaume B, Bergmann-Leitner ES, Leitner WW, Robert EG, Catez F, Smith CL, Youle RJ. The role of dynamin-related protein 1, a mediator of mitochondrial fission, in apoptosis. Dev Cell. 2001; 1:515–525. [PubMed: 11703942]
15. Frederick RL, Shaw JM. Moving mitochondria: establishing distribution of an essential organelle. Traffic. 2007; 8:1668–1675. [PubMed: 17944806]
16. Giedt RJ, Yang C, Zweier JL, Matzavinos A, Alevriadou BR. Mitochondrial fission in endothelial cells after simulated ischemia/reperfusion: role of nitric oxide and reactive oxygen species. Free Radic Biol Med. 2012; 52:348–356. [PubMed: 22100972]
17. Gonzalez, RC.; Woods, RE. Digital Image Processing. 3. Pearson Prentice Hall; Upper Saddle River, NJ: 2008.
18. Gottlob K, Majewski N, Kennedy S, Kandel E, Robey RB, Hay N. Inhibition of early apoptotic events by Akt/PKB is dependent on the first committed step of glycolysis and mitochondrial hexokinase. Genes Dev. 2001; 15:1406–1418. [PubMed: 11390360]
19. Guillery O, Malka F, Frachon P, Milea D, Rojo M, Lombes A. Modulation of mitochondrial morphology by bioenergetics defects in primary human fibroblasts. Neuromuscul Disord. 2008; 18:319–330. [PubMed: 18395446]
20. Hahn-Windgassen A, Nogueira V, Chen CC, Skeen JE, Sonenberg N, Hay N. Akt activates the mammalian target of rapamycin by regulating cellular ATP level and AMPK activity. J Biol Chem. 2005; 280:32081–32089. [PubMed: 16027121]
21. Hansen, C.; Nagy, JG.; O'Leary, DP. Deblurring Images - Matrices, Spectra, and Filtering. Society for Industrial and Applied Mathematics (SIAM); Philadelphia, PA: 2006.
22. Haralick, RM.; Shapiro, LG. Computer and Robot Vision. Vol. I. Addison-Wesley; Reading, MA: 1992.
23. Hollenbeck PJ, Saxton WM. The axonal transport of mitochondria. J Cell Sci. 2005; 118:5411–5419. [PubMed: 16306220]
24. Jahani-Asl A, Germain M, Slack RS. Mitochondria: Joining forces to thwart cell death. Biochim Biophys Acta. 2010; 1802:162–166. [PubMed: 19747972]
25. Jaqaman K, Loerke D, Mettlen M, Kuwata H, Grinstein S, Schmid SL, Danuser G. Robust single-particle tracking in live-cell time-lapse sequences. Nat Methods. 2008; 5:695–702. [PubMed: 18641657]

26. Jendrach M, Mai S, Pohl S, Voth M, Bereiter-Hahn J. Short- and long-term alterations of mitochondrial morphology, dynamics and mtDNA after transient oxidative stress. Mitochondrion. 2008; 8:293–304. [PubMed: 18602028]
27. Kuznetsov AV, Hermann M, Saks V, Hengster P, Margreiter R. The cell-type specificity of mitochondrial dynamics. Int J Biochem Cell Biol. 2009; 41:1928–1939. [PubMed: 19703655]
28. Lee YJ, Jeong SY, Karbowski M, Smith CL, Youle RJ. Roles of the mammalian mitochondrial fission and fusion mediators Fis1, Drp1, and Opa1 in apoptosis. Mol Biol Cell. 2004; 15:5001–5011. [PubMed: 15356267]
29. Liu X, Hajnoczky G. Altered fusion dynamics underlie unique morphological changes in mitochondria during hypoxia-reoxygenation stress. Cell Death Differ. 2011; 18:1561–1572. [PubMed: 21372848]
30. McBride HM, Neuspiel M, Wasiak S. Mitochondria: more than just a powerhouse. Curr Biol. 2006; 16:R551–560. [PubMed: 16860735]
31. Meeusen S, McCaffery JM, Nunnari J. Mitochondrial fusion intermediates revealed in vitro. Science. 2004; 305:1747–1752. [PubMed: 15297626]
32. Misko A, Jiang S, Wegorzewska I, Milbrandt J, Baloh RH. Mitofusin. 2 is necessary for transport of axonal mitochondria and interacts with the Miro/Milton complex. J Neurosci. 2010; 30:4232–4240. [PubMed: 20335458]
33. Mitra K, Wunder C, Roysam B, Lin G, Lippincott-Schwartz J. A hyperfused mitochondrial state achieved at G1-S regulates cyclin E buildup and entry into S phase. Proc Natl Acad Sci U S A. 2009; 106:11960–11965. [PubMed: 19617534]
34. Muller M, Mironov SL, Ivannikov MV, Schmidt J, Richter DW. Mitochondrial organization and motility probed by two-photon microscopy in cultured mouse brainstem neurons. Exp Cell Res. 2005; 303:114–127. [PubMed: 15572032]
35. Pletjushkina OY, Lyamzaev KG, Popova EN, Nepryakhina OK, Ivanova OY, Domnina LV, Chernyak BV, Skulachev VP. Effect of oxidative stress on dynamics of mitochondrial reticulum. Biochim Biophys Acta. 2006; 1757:518–524. [PubMed: 16829229]
36. Qian H, Sheetz MP, Elson EL. Single particle tracking. Analysis of diffusion and flow in two-dimensional systems. Biophys J. 1991; 60:910–921. [PubMed: 1742458]
37. Rambold AS, Kostelecky B, Elia N, Lippincott-Schwartz J. Tubular network formation protects mitochondria from autophagosomal degradation during nutrient starvation. Proc Natl Acad Sci U S A. 2011
38. Saotome M, Safiulina D, Szabadkai G, Das S, Fransson A, Aspenstrom P, Rizzuto R, Hajnoczky G. Bidirectional Ca^{2+}-dependent control of mitochondrial dynamics by the Miro GTPase. Proc Natl Acad Sci U S A. 2008; 105:20728–20733. [PubMed: 19098100]
39. Saunter CD, Perng MD, Love GD, Quinlan RA. Stochastically determined directed movement explains the dominant small-scale mitochondrial movements within non-neuronal tissue culture cells. FEBS Lett. 2009; 583:1267–1273. [PubMed: 19265695]
40. Sauvanet C, Duvezin-Caubet S, di Rago JP, Rojo M. Energetic requirements and bioenergetic modulation of mitochondrial morphology and dynamics. Semin Cell Dev Biol. 2010; 21:558–565. [PubMed: 20025987]
41. Saxton MJ, Jacobson K. Single-particle tracking: applications to membrane dynamics. Annu Rev Biophys Biomol Struct. 1997; 26:373–399. [PubMed: 9241424]
42. Sedgewick, R. Algorithms in C, Parts 1–4. 3. Addison-Wesley; Reading, MA: 1998.
43. Song W, Bossy B, Martin OJ, Hicks A, Lubitz S, Knott AB, Bossy-Wetzel E. Assessing mitochondrial morphology and dynamics using fluorescence wide-field microscopy and 3D image processing. Methods. 2008; 46:295–303. [PubMed: 18952177]
44. Soubannier V, McBride HM. Positioning mitochondrial plasticity within cellular signaling cascades. Biochim Biophys Acta. 2009; 1793:154–170. [PubMed: 18694785]
45. Tondera D, Grandemange S, Jourdain A, Karbowski M, Mattenberger Y, Herzig S, Da Cruz S, Clerc P, Raschke I, Merkwirth C, Ehses S, Krause F, Chan DC, Alexander C, Bauer C, Youle R, Langer T, Martinou JC. SLP-2 is required for stress-induced mitochondrial hyperfusion. EMBO J. 2009; 28:1589–1600. [PubMed: 19360003]

46. Widlansky ME, Gutterman DD. Regulation of endothelial function by mitochondrial reactive oxygen species. Antioxid Redox Signal. 2011; 15:1517–1530. [PubMed: 21194353]

47. Yi M, Weaver D, Hajnoczky G. Control of mitochondrial motility and distribution by the calcium signal: a homeostatic circuit. J Cell Biol. 2004; 167:661–672. [PubMed: 15545319]

48. Yoon YS, Yoon DS, Lim IK, Yoon SH, Chung HY, Rojo M, Malka F, Jou MJ, Martinou JC, Yoon G. Formation of elongated giant mitochondria in DFO-induced cellular senescence: involvement of enhanced fusion process through modulation of Fis1. J Cell Physiol. 2006; 209:468–480. [PubMed: 16883569]

49. Youle RJ, Karbowski M. Mitochondrial fission in apoptosis. Nat Rev Mol Cell Biol. 2005; 6:657–663. [PubMed: 16025099]

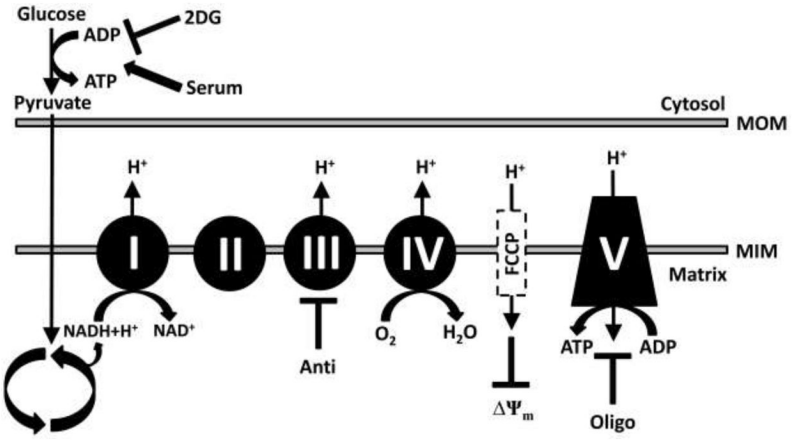

Fig. 1.

Schematic representation of the different compounds' target in the OXPHOS/glycolysis pathway: FCCP, an OXPHOS uncoupler that dissipates $\Delta\Psi_m$; antimycin A (abbreviated as Anti), a complex III inhibitor; oligomycin (abbreviated as Oligo), an ATP synthase inhibitor; 2DG, a glycolysis inhibitor; and serum, an activator of glycolysis/OXPHOS (modified from Guillery et al.[19]).

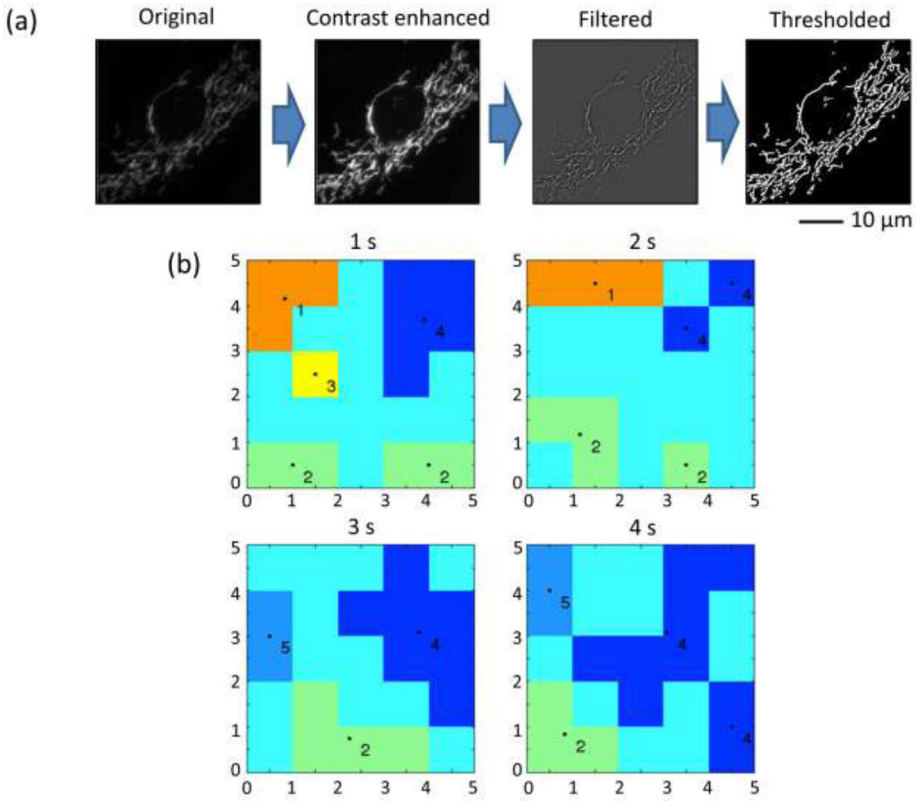

Fig. 2.

Image processing and mitochondrial dynamics analysis. (a) Characteristic processing sequence of an original image (video frame) showing an EC transduced with mito-GFP. Each original image was contrast enhanced and filtered to improve structural definition. The image was then thresholded resulting in a binarized image, where mitochondrial objects were white on a black background. (b) Matlab analysis was employed to track objects in each binarized image creating a 3D label matrix. A simplified label matrix with a size of (5,5,4), broken down to 2D segments for every s up to 4 s, is shown. The algorithm identified objects at each time frame, tracked their shapes/centroids, and identically pseudo colored those that interacted at some time point in the video.

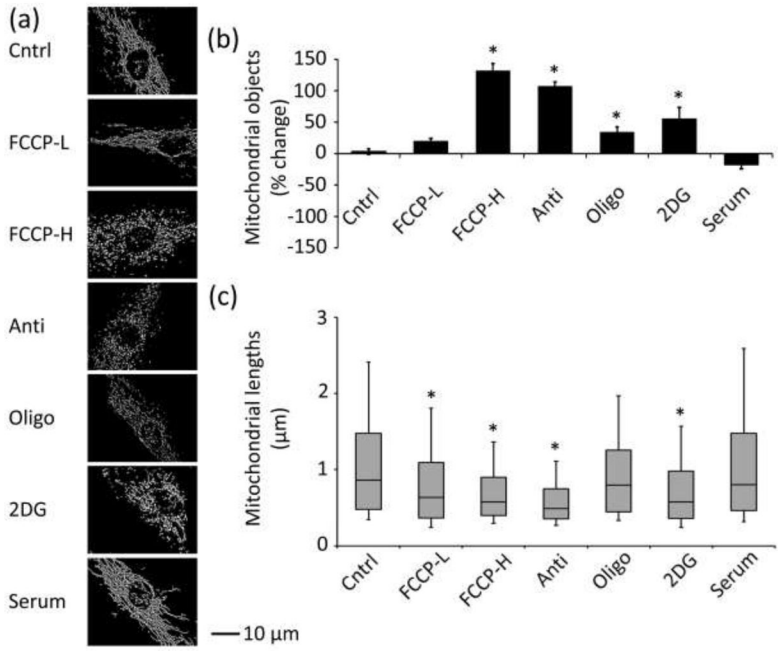

Fig. 3.

EC mitochondrial morphology changes due to bioenergetic stress. (a) Characteristic binarized images of ECs transduced with mito-GFP and treated, or not, with FCCP, antimycin A, oligomycin, 2DG or serum. (b) Percentage change in total mitochondrial object count at 30 min following treatment compared to corresponding controls (prior to treatment). (c) Box plot showing the $90^{th}/10^{th}$ (lines) and $25^{th}/75^{th}$ percentiles (filled bars) and medians (center lines) of mitochondrial length for each treatment (>100 images were analyzed from n≥3 independent experiments per treatment). *P<0.05 relative to control.

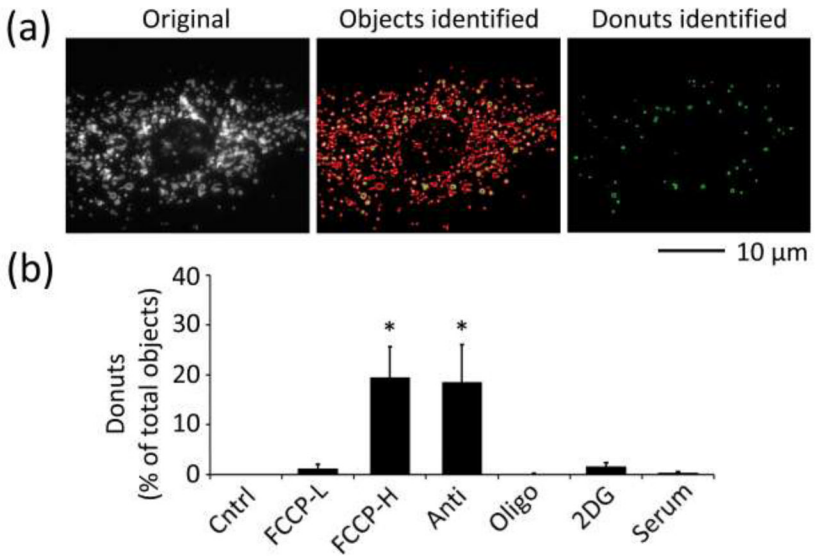

Fig. 4.

EC mitochondrial donut analysis. (a) A characteristic original image of an EC showing donut-shaped mitochondria was analyzed to identify all objects (outlined in red) and only the donuts (outlined in green). (b) Percentage of total objects identified as donuts. For each treatment, >100 images were analyzed from n≥3 independent experiments. *P<0.05 relative to control.

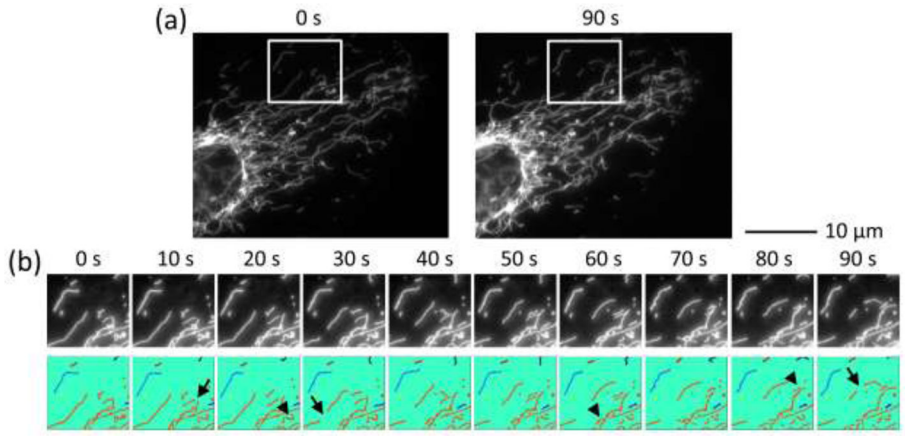

Fig. 5.

Digital image analysis of a characteristic control video. (a) Video of an EC, transduced with mito-GFP and prior to any treatment (control), was acquired for 90 s; only the 0 and 90 s time frames with a cropped region inset (white box) are shown. (b) On the top row, contrast enhanced time frames of the cropped region in 10 s intervals; on the bottom row, corresponding Matlab results (objects on a green background; interacting objects identified by identical color). Arrows and arrowheads were added for the purpose of demonstrating the occurrence of fission and fusion events, respectively, during the video.

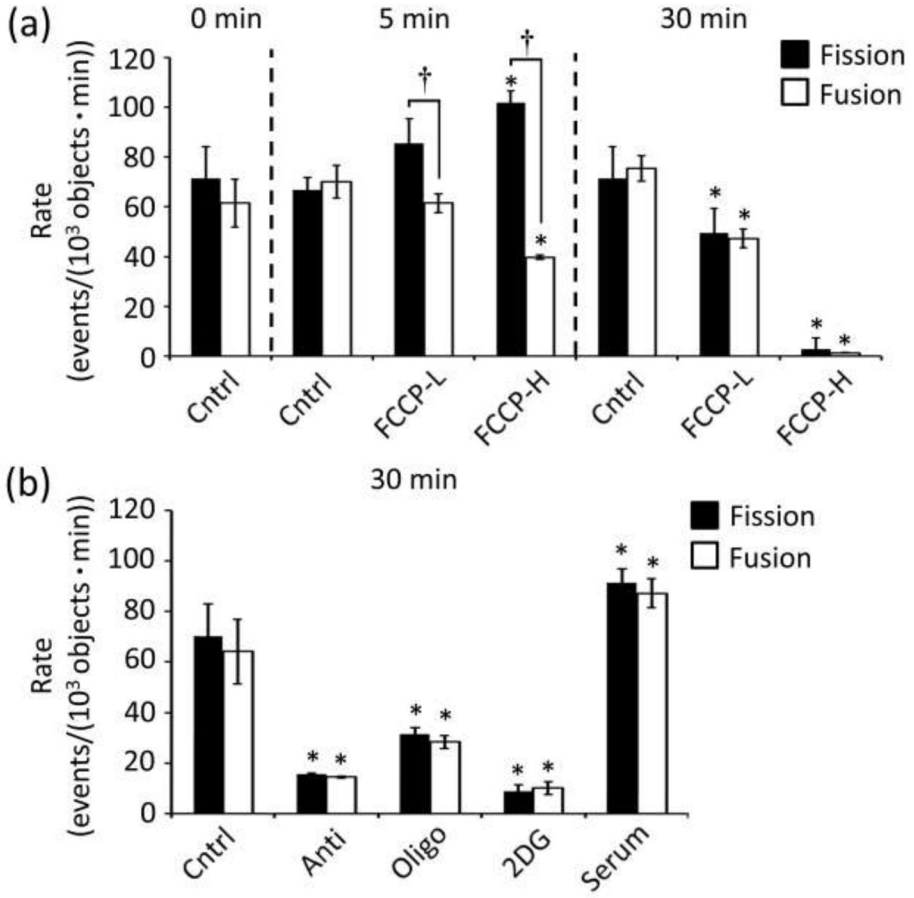

Fig. 6.

Mitochondrial fission and fusion rates of ECs exposed to bioenergetic stress. (a) Fission and fusion rates in control ECs and ECs treated with FCCP-L and -H for 0, 5 and 30 min. (b) Fission and fusion rates in control ECs and ECs treated with antimycin A, oligomycin, 2DG or serum for 30 min. At least 10 cropped videos were analyzed from n≥3 independent experiments per treatment. *P<0.05 relative to respective control. †P<0.05 for a comparison between fission and fusion rates at the same time/condition.

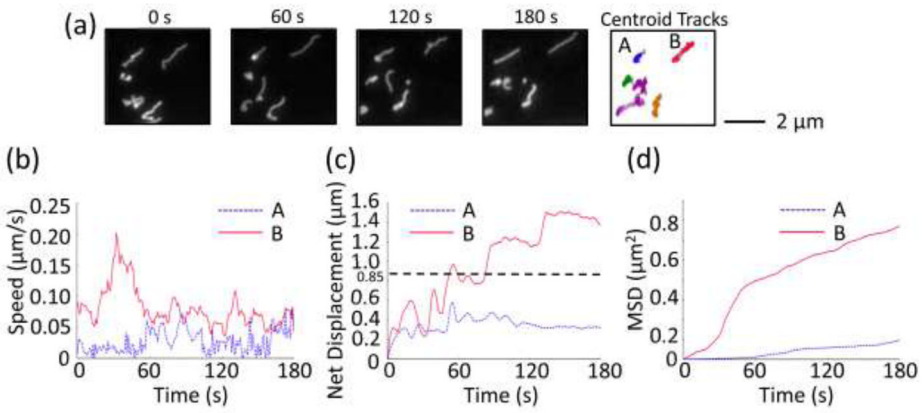

Fig. 7.

EC mitochondrial motility changes due to bioenergetic stress. (a) Object centroids were tracked in a cropped video of 180 s showing examples of movement without a burst in displacement (object A; blue tracks) and movement with a burst in displacement (object B; red tracks). (b) Speed (at every s) versus time for the two objects studied, object A (blue dotted line) and object B (red solid line). (c) Net displacement versus time for the two objects studied. The horizontal dotted line indicates that the net displacement of B exceeded 0.85 μm within 1 min of tracking, allowing us to categorize B as an object that underwent a "step" motion. (d) Corresponding MSD versus time plots for the two objects studied.

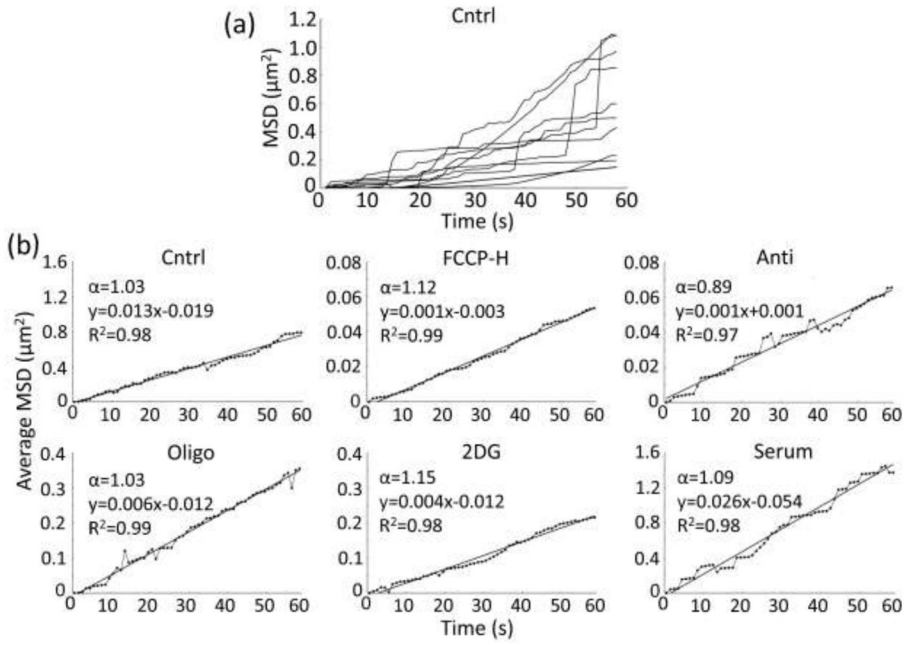

Fig. 8.

Mathematical analysis of MSDs and characterization of mitochondrial motion. (a) Experimentally measured MSD vs. time profiles for 10 randomly selected mitochondrial objects in a control EC and 1 min of tracking. (b) Average MSD (of >100 objects from n≥3 independent experiments) vs. time profiles for control, FCCP-H, antimycin A, oligomycin, 2DG and serum. In each case, the α value, linear curve fit and its equation, and R^2 value are shown.

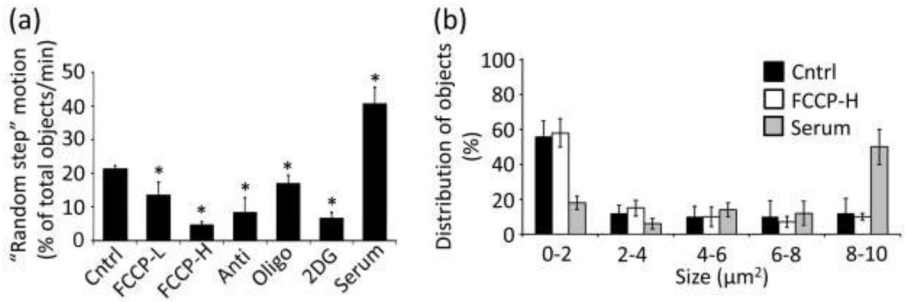

Fig. 9.

Changes in the "random step" mitochondrial motion due to bioenergetic stress. (a) Percentage of mitochondrial objects undergoing bursts in displacement (leading to a net displacement of >0.85 μm per min of tracking) for each condition tested. *P<0.05 relative to control. (b) Objects that underwent bursts in displacement, in control, FCCP-H and serum treated ECs, were binned according to size. For a and b, >100 objects were analyzed from n≥3 independent experiments per treatment.

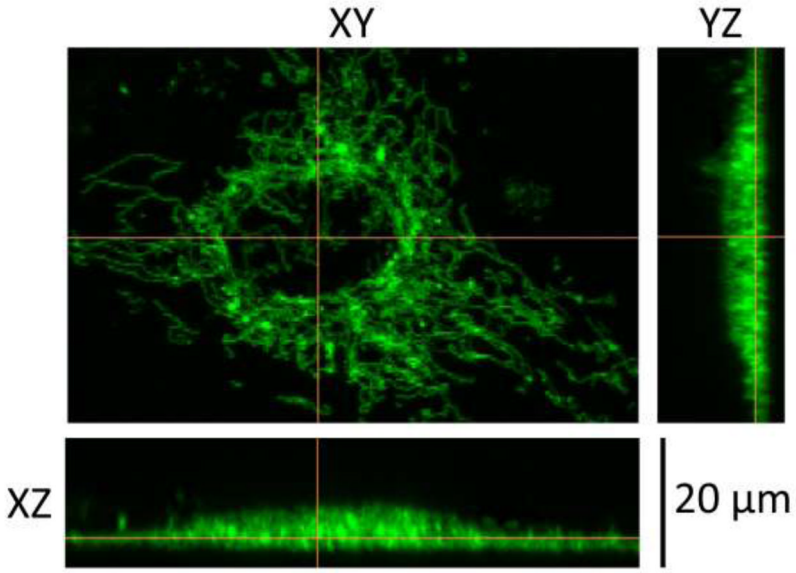

Fig. 10.

Representative 3D reconstruction (Z-stack) from a control EC viewed by confocal fluorescence microscopy (100x magnification). 41 Z slices were acquired every 0.5 μm covering a total height of 20 μm. From the XZ and YZ projections, it was concluded that the height of the mitochondrial network in the cell periphery is ≤4 μm.